PNNL-12240, Rev. 0

Pacific Northwest
National Laboratory
Operated by Battelle for the
U.S. Department of Energy

Evaluation of the Long-Term Performance of Titanate Ceramics for Immobilization of Excess Weapons Plutonium: Results From Pressurized Unsaturated Flow and Single Pass Flow-Through Testing

B. P. McGrail
J. P. Icenhower
V. L. Legore
P. F. Martin
H. T. Schaef
R. D. Orr

July 1999

Prepared for the U.S. Department of Energy
under Contract DE-AC06-76RLO 1830

DISCLAIMER

PACIFIC NORTHWEST NATIONAL LABORATORY
operated by
BATTELLE MEMORIAL INSTITUTE
for the
UNITED STATES DEPARTMENT OF ENERGY
under Contract DE-AC06-76RLO 1830

Printed in the United States of America

Available to DOE and DOE contractors from the Office of Scientific and Technical Information, P.O. Box 62, Oak Ridge, TN 37831; prices available from (615) 576-8401.

Available to the public from the National Technical Information Service, U.S. Department of Commerce, 5285 Port Royal Rd., Springfield, VA 22161

Evaluation of the Long-Term Performance of Titanate Ceramics For Immobilization of Excess Weapons Plutonium: Results From Pressurized Unsaturated Flow and Single Pass Flow-Through Testing

B. P. McGrail
P. F. Martin
J. P. Icenhower
H. T. Schaef
V. L. Legore
R. D. Orr

July 1999

Prepared for
the U.S. Department of Energy
under Contract DE-AC06-76RLO 1830

Pacific Northwest National Laboratory
Richland, Washington 99352

DISCLAIMER

Portions of this document may be illegible in electronic image products. Images are produced from the best available original document.

SUMMARY

This report summarizes our findings from pressurized unsaturated flow (PUF) and single-pass flow-through (SPFT) experiments to date. Results from the PUF test of a Pu-bearing ceramic with enclosing surrogate high-level waste glass show that the glass reacts rapidly to alteration products. Glass reaction causes variations in the solution pH in contact with the ceramic materials. We also document variable concentrations of Pu in solution, primarily in colloidal form, which appear to be related to secular variations in solution composition. The apparent dissolution rate of the ceramic waste form, based on Ba concentrations in the effluent, is estimated at $\leq 10^{-5}$ g/(m^2·d). Pu-bearing colloids were recovered in the size range of 0.2 to 2 μm, but it is not clear that such entities would be transported in a system that is not advective-flow dominated.

Results from SPFT experiments give information on the corrosion resistance of two surrogate Pu-ceramics (Ce-pyrochlore and Ce-zirconolite) at 90°C over a pH range of 2 to 12. The two ceramics were doped with minor quantities (~0.1 mass%) of MoO_3, so that concentrations of Mo in the effluent solution could be used to monitor the reaction behavior of the materials. The data obtained thus far from experiments with durations up to 150 d do not conclusively prove that the solid-aqueous solution systems have reached steady-state conditions. Therefore, the dissolution mechanism cannot be determined. Apparent dissolution rates of the two ceramic materials based on Ce, Gd, and Mo concentrations in the effluent solutions from the SPFT are nearly identical and vary between 1.1 to 8.5×10^{-4} g/(m^2·d). In addition, the data reveal a slightly amphoteric dissolution behavior, with a minimum apparent rate at pH = 7 to 8, over the pH range examined.

Results from two related ceramic samples suggest that radiation damage can have a measurable effect on the dissolution of titanium-based ceramics. The rare earth pyrochlores, $Gd_2Ti_2O_7$ and $Lu_2Ti_2O_7$, are being studied as part of the DOE Environmental Management Science Program, and the results are germane to this study. The corrosion resistances of both heavy-ion bombarded and pristine (non-bombarded) specimens are being examined with the SPFT test. Initial data indicate that the dissolution rate may increase by a factor of 3 times or more when these materials become amorphous from radiation damage.

For both the SPFT and PUF tests, data and specimen characterization are continuing.

CONTENTS

INTRODUCTION

The U.S. Department of Energy Office of Fissile Material Disposition has indicated that the ceramic can-in-canister design is the preferred option for the disposal of surplus weapons Pu in the proposed, mined geologic repository at Yucca Mountain, Nevada [1]. The long-term release of ^{239}Pu, ^{235}U, and neutron absorbers from the ceramic in this can-in-canister configuration must be understood before a credible safety analysis can be conducted. The credible scenarios for the degradation of the ceramic all involve ground water. From a repository point of view, the fastest release of material from the waste form provides the worst case for release of components. This information comes from the single-pass flow-through (SPFT) test. Information on how the alteration of the high-level waste glass affects the alteration and concomitant release of components from the Pu-bearing ceramic is provided by the pressurized unsaturated flow (PUF) test. Results from both of these tests are discussed in this report.

At some time in the distant future, water is expected to penetrate the waste containers and contact the waste forms. Although several scenarios of water contact are possible, the most credible contact mode from a hydraulics viewpoint is the slow percolation of water through the waste packages under conditions of partial hydraulic saturation. Gravity and capillary forces drive flow through the containers. Because the can-in-canister waste packages are expected to contain approximately 85 vol% of HLW glass and 15 vol% of Pu-bearing ceramic, any water percolating through the containers will react chemically with both high-level waste (HLW) glass and the Pu ceramic. Although exact flow paths through a waste package are not known, the substantially higher amount of glass compared with ceramic suggests that on average, water will contact glass before contacting ceramic. The glass is also expected to react faster than the ceramic and to contain a significant amount of exchangeable cations, which are subject to diffusive and advective mass transport. For all these reasons, the glass is expected to dominate the chemistry of any water percolating through a can-in-canister waste package. Consequently, it is important to understand how the glass/water reaction impacts, if at all, corrosion of the ceramic and the release and transport behavior of Pu and the neutron absorbers. In this report, we summarize the results from a 17-month experiment utilizing PUF system at Pacific Northwest National Laboratory (PNNL).

The dissolution kinetics of two pyrochlore ceramic samples were investigated through the use of SPFT experiments over a pH-interval of 2-12 at 90°C temperature. Although static (such as the PCT and MCC) tests are widely used to determine the behavior of waste form-aqueous solution systems under repository conditions, SPFT experiments are ideal for elucidating the kinetic parameters that will be used to model release rates from the waste package. The usefulness of SPFT results stem from the fact that effluent solutions have low concentrations of dissolved constituents thereby keeping the system at low, and ideally, constant, chemical affinities (or reaction progress). Another useful property of flow-through systems is that the continuous replacement of solution in the reactor allows the solution to remain at constant pH, which minimizes uncertainties in the reaction rates. In addition, many mineral- or glass-solution systems reach a steady-state condition over time, which allows the investigator to retrieve a number of important kinetic parameters that can be used to effectively model release rates of radionuclides into the geosphere.

Over the last few decades a general rate equation, based on Transition State Theory, has been fashioned to described the dissolution of glass and silicate minerals into aqueous solution:

$$k = k_o \nu_i a_{H^+}^{-\eta} e^{\frac{-E_a}{RT}} \left[1 - \left(\frac{Q}{K}\right)^{\sigma}\right] \prod_j a_j^{-\eta_j} \qquad (1)$$

where: k = dissolution rate, g/(m^2·d)

k_o = intrinsic rate constant, g/(m^2·d)

ν_i = the stoichiometric coefficient of element i in the ceramic (dimensionless)

a_{H^+} = hydrogen ion activity, mol/L

a_j = activity of the jth aqueous species, mol/L

E_a = activation energy, kJ/mol

R = gas constant, kJ/(mol· K)

T = temperature, K

Q = ion activity product

K = equilibrium constant

η = power law coefficient

σ = Temkin coefficient.

The test conditions of our SPFT experiments are designed such that the value of Q/K is nearly zero. If this approach proves to be valid, we will be able to recover many of the parameters that will be useful to radionuclide release models. However, as the value of K for titanate-based ceramics is essentially unknown, it is not yet possible to conclusively demonstrate that this condition is achieved. In addition, it is not known whether the activities of other aqueous species (besides H^+) impact the dissolution rate of pyrochlore minerals.

Note, however, that even if this approach fails, we can still recover important data that will prove decisive in long-term performance assessments of this material. By varying temperature and solution pH, the activation energy (E_a) and the pH power law coefficient (η) can be determined. Determining the activation energy of reaction is an important component of the SPFT tests because it can distinguish between mechanisms that are likely to control dissolution. For example, typical activation energies for diffusion-controlled dissolution (10 to 20 kJ/mol) are much smaller than those for surface reaction-dominated dissolution (70 to 90 kJ/mol).

EXPERIMENTAL

The experimental methods used for both pressurized unsaturated flow (PUF) and single-pass flow-through (SPFT) tests are described in this section.

PUF TEST

Because the purpose of this test is to determine if the chemical changes in water that has reacted with HLW glass alters the corrosion rate of the ceramic or release and transport of Pu and the neutron absorbers, a "sandwich" configuration, as illustrated in Figure 1, was selected. To match the approximate volumes of glass and ceramic in a can-in-canister configuration, 85% of the volume was allocated for glass (42.5% in the top and bottom beds) and 15% with ceramic. Details on the glass and ceramic materials used are given in the Materials section. Details on the PUF system are discussed next.

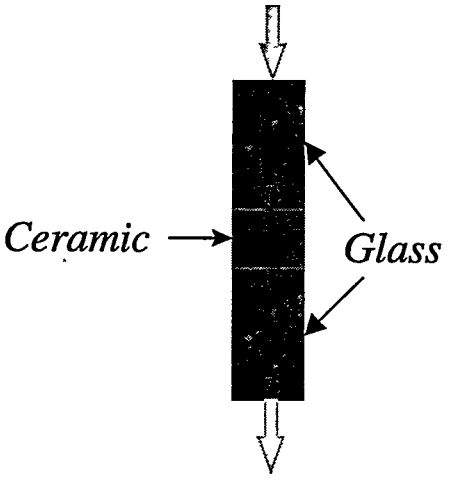

Figure 1. Schematic of PUF Interaction Test

PUF SYSTEM

The PUF system has been discussed in detail elsewhere [2,3], but is briefly described here. The experimental design provides a novel way to study waste form corrosion behavior under unsaturated conditions, subject to open-system flow and transport. The basic test apparatus consists of a column packed with particles of the test material or materials of a known size and density, and a computer data acquisition and control system (Figure 2). The column is fabricated from a chemically inert material (polyetheretherketone) so that dissolution reactions are not influenced by interaction with the column. A porous titanium plate with nominal pore size of 0.2 μm is sealed in the bottom of the column to ensure an adequate pressure differential for the conductance of fluid while operating under unsaturated conditions [4]. Titanium was chosen because it is highly corrosion resistant and has excellent wetting properties. When water saturated, the porous plate allows water but not air to flow through it, as long as the applied pressure differ-

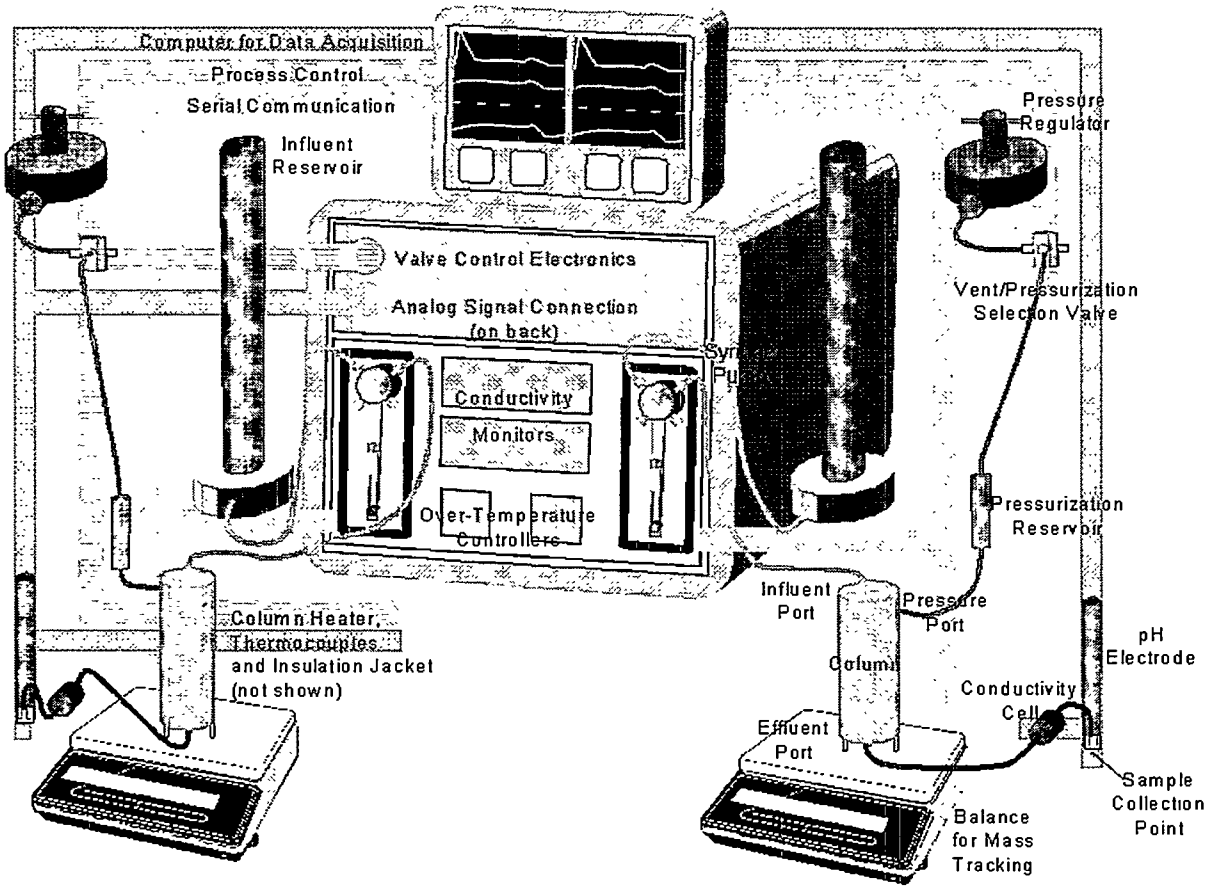

Figure 2. Schematic of PUF Test System (patent allowed)

ential does not exceed the air entry relief pressure, or "bubble pressure," of the plate. The computer control system runs LabVIEW™ (National Instruments Corporation, Austin, Texas) software for logging test data to disk from several thermocouples, pressure sensors, inline sensors for effluent pH and conductivity, and column weight from an electronic balance to accurately track water mass balance and saturation level. The column also includes a proprietary "PUF port," which is an electronically actuated valve that periodically vents the column gases at an interval specified by the operator. The purpose of column venting is to prevent reduction in the partial pressure of important gases, especially O_2 and CO_2 that are participants in a variety of homogeneous and heterogeneous chemical reactions.

MATERIALS

The ceramic used in this test (CPSF5) was produced at Lawrence Livermore National Laboratory and shipped to PNNL. The target composition was 80 mass% zirconolite with 15 mass% Ba-hollandite and 5 mass% rutile. The ceramic was made with 16 mass% PuO_2 and doped approximately equimolar with Gd. The starting components were wet mixed in a ball mill for about 1 hour. The material was dried overnight in a convection oven. The dried material was then calcined at 600°C for 1 hour. The calcined precursor material was dry mixed in a V-shell mixer and 318.5 g was blended with 50.0 g of PuO_2. The PuO_2 was "high-fired" material, i.e. calcined at 1000°C for four hours. The PuO_2 was ground in a mortar and pestle then sieved through a 20-μm screen (600 mesh). Material passing through the sieve was used as the feed material. The ceramic powder was pressed at approximately 0.14 MPa (20 000 psi) in a 8.9 cm diameter die. The pellet was heated to around 300°C for several hours. The sample cracked into three pieces, presumably due to the presence of the binder and a heating rate that was too fast. The material was recovered, reground, repressed again at about 0.14 MPa. The pellet was heated again to 300°C for about 10 hours then sintered at 1300°C for about 4 hrs. The final product was fractured into two pieces and annealed twice at 1350°C for about 5 hours. The CPSF5 ceramic is an early formulation and differs from the current baseline ceramic composition in that current ceramic does not contain Ba (as Ba-hollandite), and contains Hf and U instead of Zr. Nevertheless, the corrosion behaviors of the Pu-bearing phases in both the old and current formulations are expected to be similar, and the effects of glass corrosion on the release of components from the ceramic should be quite comparable.

Table 1. Target Composition for CPSF5

Oxide	Mass%
ZrO_2	17.91
TiO_2	40.85
Gd_2O_3	8.83
CaO	8.15
Al_2O_3	8.15
BaO	3.40
PuO_2	16.11

A simulated HLW glass was used in the PUF experiment. Approximately 2 kg of glass was received from the Savannah River Technology Center labeled WP-14. The glass was chipped from a canister of glass that had been produced as part of a cold demonstration at the Defense Waste Processing Facility. Staff at SRTC transmitted a chemical analysis of the glass, which is given in Table 2.

Crushed glass and ceramic were prepared following the procedure detailed by the American Society for Testing and Materials [5]. The materials were ball milled and sieved to separate the 850 to 212 μm (-20+70 mesh) size fraction. The crushed and sieved material was then washed ultrasonically with demineralized water and ethanol to remove fines, and then dried. Representative samples of the crushed, sieved, and washed samples were surveyed with a scanning electron microscope (SEM) to verify that the size of the grains was consistent with the sieved size fraction and that fines had been removed. The specific surface area of the crushed samples was estimated by assuming the particles to be spheres having radii equal to the average opening of the sieves [6]. The Archimedes method was used to measure bulk density; the WP-14 glass was measured to be 2710 ±50 kg/m^3, giving a specific surface area of 0.0042 m^2/g. The density of the ceramic was measured to be 4480 ±110 kg/m^3 giving a specific surface area of 0.0025 m^2/g.

Table 2. Analyzed Composition of WP-14 Glass

Oxide	Mass%	
Al_2O_3	4.71	±0.042
B_2O_3	6.91	±0.058
CaO	1.10	±0.028
Cr_2O_3	0.33	±0.026
CuO	0.36	±0.006
Fe_2O_3	12.40	±0.135
K_2O	1.99	±0.049
Li_2O	4.48	±0.044
MgO	1.49	±0.017
MnO_2	3.23	±0.070
Na_2O	7.82	±0.136
Nd_2O_3	0.35	±0.019
NiO	1.05	±0.029
PbO	0.16	±0.005
SiO_2	50.92	±0.406
TiO_2	0.24	±0.004
ZnO	0.09	±0.002
ZrO_2	1.19	±0.025
Total	98.83	±1.100

PUF TEST PROCEDURE

The PUF column with an internal volume of 21.72 cm^3 was packed first with ½ the total required crushed and cleaned WP-14 glass, then with the crushed and cleaned CPSF5 ceramic, and finally with the remaining WP-14 glass. The mass difference between the full and empty column was used to calculate the initial porosity of approximately 0.46 ±0.02. Mass change and bed volume were also tracked during packing of each layer to compute the porosity for each layer. Individual bed porosity was within the reported measurement error above. The column was then vacuum saturated with water at ambient temperature. A temperature controller was programmed to heat the column to 90°C in approximately 1 h (1°C/min). The column was allowed to desaturate initially during heating by gravity drainage and was also vented periodically to maintain an internal pressure less than the bubble pressure of the porous plate. After reaching 90°C, the influent valve was opened, and influent set to a flow rate of 1 mL/d. Column venting was set to occur once an hour. Effluent samples were collected in a receiving vessel that was drained

nominally on a 5-day interval but sometimes more often when changes in the effluent pH and conductivity were detected. The samples were drained into tared vials from which samples were extracted and acidified for elemental analysis with ICP-MS. The ICP-MS was calibrated with certified standards prior to each series of analyses.

Liquid scintillation counting (LSC) was used for the analysis of alpha and beta emitting isotopes. Due to the nature of the LSC method, all alpha emitting isotopes appear at roughly the same energy and intensity spectrographically. The samples were analyzed, therefore, under the assumption that all alpha activity in the sample was contributed from ^{239}Pu and ^{241}Am. The ^{241}Pu low energy beta peak is quite well resolved spectrographically by the LSC method. After LSC analysis, the samples were analyzed for ^{241}Am with gamma energy analysis (GEA). Americium-241 has a 59.5 keV photon of relatively high abundance, whereas the contribution of photons from all isotopes of Pu is negligible. The ^{241}Am activity determined with GEA was then used to correct the total alpha activity determined with LSC to obtain the ^{239}Pu activity.

During the course of the experiment, several effluent samples were filtered through Centricon 30 ultrafiltration cones (30 000 molecular weight cutoff, or approximately 1.8 nm particle size). As will be discussed later, the results showed that most of the Pu in the effluent was associated with filterable particles. However, because the normal sampling procedure is to collect the effluent samples in vials that are allowed to cool to room temperature, concerns were raised that precipitation of solids during cooling could have resulted in the formation of the particulate Pu and Am. To prevent this, samples were collected at temperature using a syringe pump and gas tight syringes. The syringes were maintained at the column temperature with heat tape. The temperature was controlled with the aid of a thermocouple and the same computerized control system used for the PUF columns to control power to the heat tape. Samples collected with this system were filtered as close to 90°C as possible, again through the Centricon 30 cones that had been pretreated by filtering an aliquot of cooled effluent. Some cooling (probably 10 to 20°C) occurred during sample transfer and centrifugation.

After a total run duration of 11 523 h, the PUF experiment was terminated. A comprehensive run termination and sample analysis plan was developed and executed. The column was split lengthwise with the aid of the miter box shown in Figure 3. One half of the column was subsampled as found (loose and moist particles) and the other half was allowed to air-dry in prepara-

tion for resin infiltration. For the half column with loose particles, 15 subsamples (3 subsamples contained the bulk of the Pu-doped ceramic) were obtained at 5 mm intervals. From these samples the following analyses were conducted:

1. Moisture content determination by drying in glass vials at room temperature in a sealed can with $CaSO_4$ desiccant. Samples were dried until a constant mass was obtained.
2. SEM, TEM, and XRD analyses of selected samples from the glass and ceramic layers.

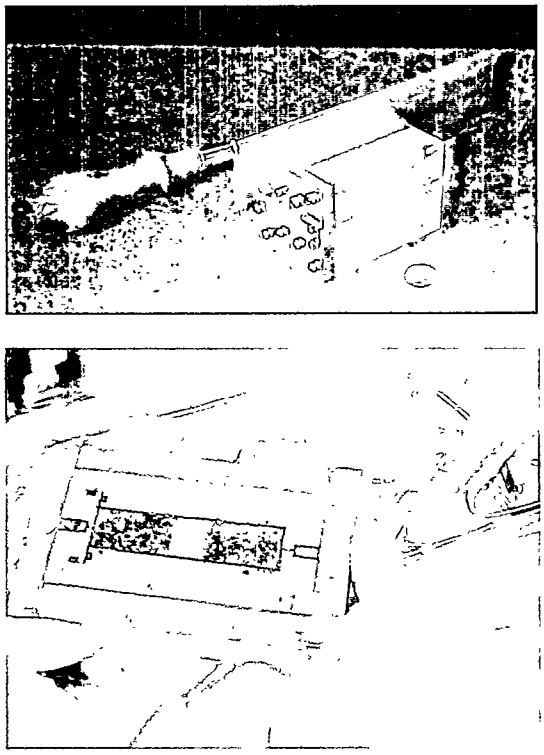

Figure 3. Schematic of Miter Box Used to Split the PUF Column and Picture of Split Column

After drying for 48 h, the other half column was impregnated with "LR White" (London Resin Co.) resin. The resin-infiltrated half-core was epoxied to a set of aluminum mounting blocks so that sections could be cut with a low-speed metallographic saw. A complete diagram illustrating the sectioning strategy employed is provided in Figure 4. The half-core was attached to the blocks on the plane that split the core along its longitudinal axis. Two initial cuts were made, perpendicular to the longitudinal axis, to separate the main bulk of the Pu-doped ceramic particles from the rest of the column bed. These initial cuts were made such that a millimeter thickness of the Pu-doped ceramic would remain attached to the WP-14 glass it had contacted while undergoing PUF testing. Three cuts were made parallel to the longitudinal axis, at approximately 2.8 mm spacings, and yielded four sets of planar samples. A set is comprised of 1) the outer curved surface of the column bed *with one cut surface*, 2) the adjacent slabs *with two cut surfaces*, and 3) the remaining thin section still adhered to aluminum mounting blocks *with one cut surface*.

It was important to wash the cut samples to remove Pu-contamination from the freshly sawn surfaces before an assessment could be made of Pu mobility under PUF flow. The two sets of the three separated samples, from the influent and effluent ends of the column, were ultrasonically washed four times for approximately five minutes in fresh deionized water. A final wash in denatured ethyl alcohol was also done. The third set of samples containing nothing but impregnated ceramic granules were saved in a vial, unwashed. The fourth thin section was also left

unwashed. Final preparation of the samples entailed splitting the slabs along their lengths thereby exposing particles uncontaminated by the cutting and cleaning process. Each of these samples was then examined with SEM and selected samples were subjected to laser ablation mass spectrometry and thin-film radiography.

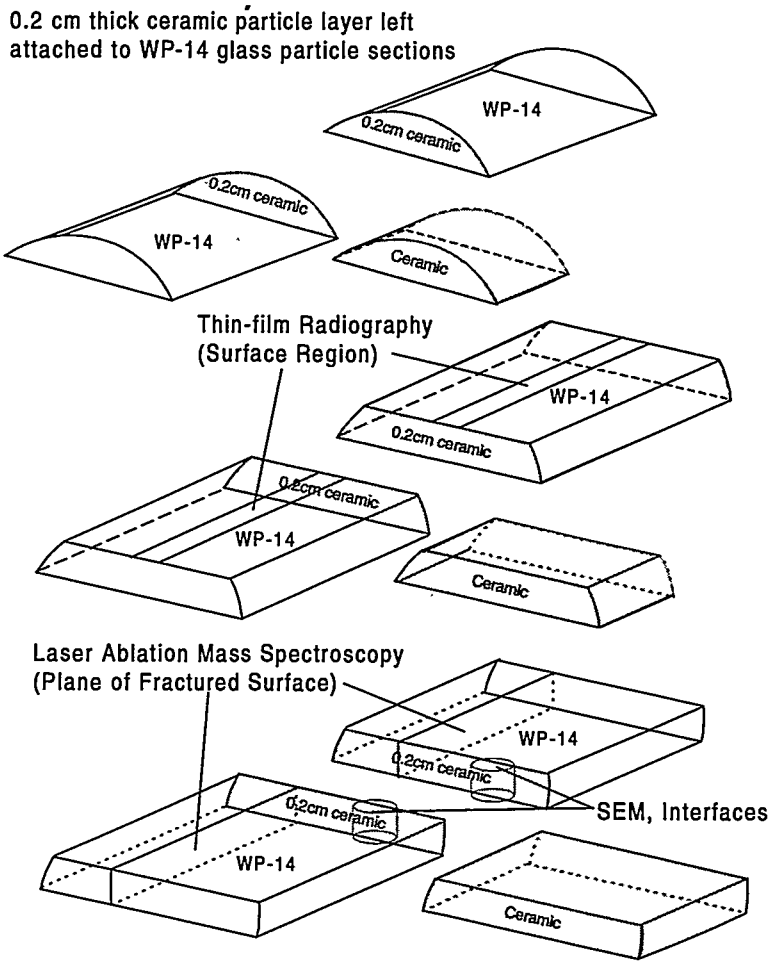

Figure 4. Schematic of Plan Used to Section Resin-Impregnated Half-Core Removed From PUF Column

SPFT TEST PROCEDURE

The SPFT system is based on the continuous movement of solution from precisely calibrated pumps, through Teflon® reactors containing the test material, and then to collection vials. Infusion or computer-controlled syringe pumps are used to control the flow rates (either 2 or 10 mL/d) in the experiments. Flow rate variations are less than 2%. Under the steady-state conditions that are established at the beginning of the experiments, the volume of fluid entering the reactor vessel is equal to the amount departing. Powdered samples of pyrochlore ceramics (either –100, +200 or –200, +325 mesh; 0.25 to 0.50 grams) are placed into a reactor and the assembly is housed in a constant temperature (90°C, ±1°C) oven. Effluent samples are collected continuously and aliquots are periodically retained for chemical analysis. Precision ICP-AES (Ca) and ICP-MS (Mo, Ce, Gd, Hf, and Ti) methods are used to determine element concentrations in the effluent. Input solutions with pH values between 2 and 12 were HNO_3, deionized water, and mixtures of nitric acid and TRIS (tris hydroxymethyl aminomethane) or lithium hydroxide and lithium chloride (see Table 3).

All input solutions are continuously sparged with nitrogen gas to prevent deviations from the initial pH values. Aliquots of the input and effluent solutions were periodically checked to document constant pH values. Typical duration of experiments is 60 to 150 days; the ongoing set of experiments has been running for approximately 90 days. Apparent dissolution rates are calculated from the expression:

Table 3. Chemical Compositions of Buffer Solutions

Buffer #	pH (25°C)	Composition
1	2	0.013 M HNO_3
2	5.7	deionized water
3	7	0.05 M TRIS + 0.0466 M HNO_3
4	8	0.05 M TRIS + 0.029 M HNO_3
5	9	0.05 M TRIS + 0.0057 M HNO_3
6	10	0.05 M TRIS + <0.150 mLs HNO_3
7	11	0.01 M LiCl and 0.001 M LiOH
8	12	0.01 M LiCl and 0.0107 M LiOH

$$rate_i = \frac{(C_i^{out} - \overline{C}_i^b)q}{f_i A} \tag{2}$$

where

$rate_i$ = the apparent dissolution rate of the ceramic sample as indexed by element i (g/(m^2·d)).

C_i^{out} = concentration of the element of interest in the effluent (µg/L).

$\overline{C}_i^b$ = average concentration of the element of interest in blank samples (µg/L).

q = solution flow-through rate (L/d)

f_i = fraction of the element in the ceramic (dimensionless).

A = surface area of the material (m^2).

Because the rate expression above is not specific to any element, an apparent dissolution rate can be calculated from a suite of elements in the effluent solution, in this case, Ti, Ca, Mo, Hf, Ce, and Gd. As will be shown below, the dissolution rates based upon the entire suite of elements yield consistent data between the samples tested. Blanks (effluent samples run through the system without ceramic powders) establish background concentrations of elements of interest in the input solution. In the cases where the concentrations of elements in the input solution are below their respective detection thresholds, the value of the detection threshold is used. The dissolution rates discussed below are all adjusted for background concentrations of the elements of interest in the input solution.

SPFT SAMPLE COMPOSITION

The chemical compositions of the Ti-pyrochlore samples used for SPFT testing are listed in Table 4. The two pyrochlore samples, Pyrochlore-12 (or PY12) and Baseline-3 (or BSL3), can be classified into the Ca-rich betafite and zirconolite subgroups, respectively. Both PY12 and BSL3 contain Ce as a surrogate for Pu. In addition, each ceramic sample was doped with a small amount of molybdenum [as Mo(VI)] that acts as a tracer of matrix dissolution. The effectiveness of molybdenum as an index of the dissolution process will be assessed below.

Table 4. Chemical Compositions (Mass%) of Ti-Ceramics

Oxide	Pyrochlore-12 (PY12)	Baseline-3 (BSL3)
CaO	8.23	11.47
CeO_2	35.38	26.84
Gd_2O_3	13.31	9.16
HfO_2	3.10	11.12
MoO_3	0.11	0.10
TiO_2	39.89	41.33
Total	100.01	100.00

RESULTS

Test results from the interactive PUF experiment with WP-14 glass and CPSF5 ceramic are presented first, followed by the results from SPFT tests.

PUF TEST RESULTS

Test Metrics

The results from the computer-monitored test metrics are shown in Figure 5a. The indicated volumetric water content becomes a less accurate indicator of pore saturation in long duration experiments because water mass may accumulate in alteration phases as waters of hydration. A check of the pre- and post-test column mass indicated a pore saturation of not more than 33.6%. This measurement was used to determine a global correction factor for the indicated pore saturation, which was applied to the volumetric water content data. The green dashed lines in Figure 5a indicate periods (about 8 h) where data acquisition was interrupted because of a software error in the control programming. A variable used in a timer subroutine overflowed when reaching 2^{32} milliseconds, which corresponds to approximately 50 days. Data acquisition was interrupted for periods of about 8 hours. Fluid flow, however, was only affected twice, once at 133 d and the other at 233 d. The software bug was discovered and corrected after the interruption at 233 d.

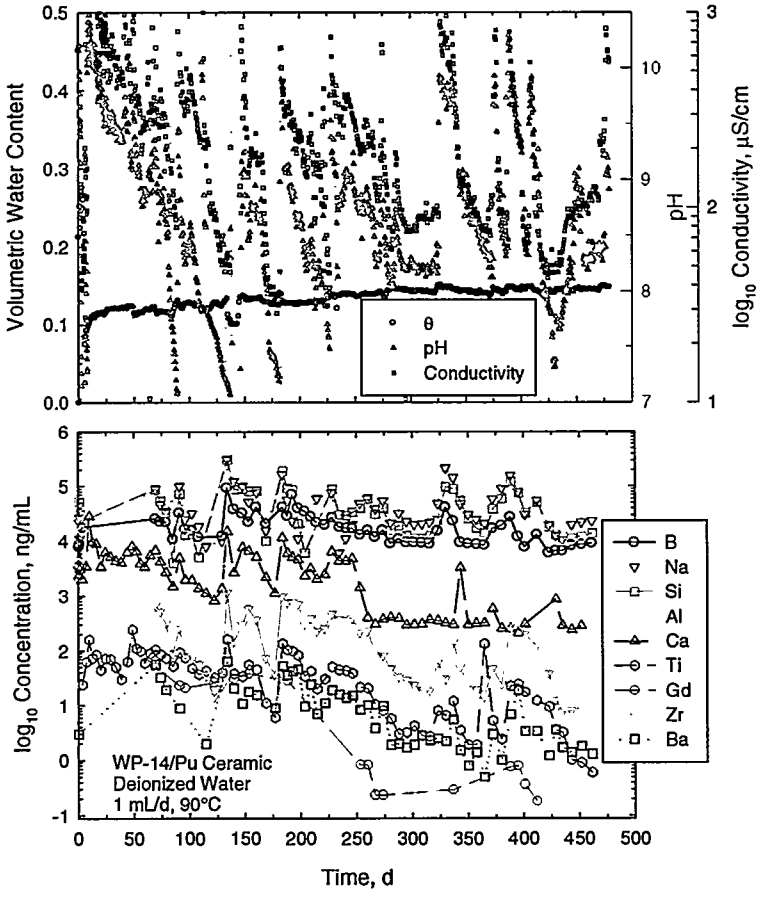

Figure 5. Computer-Monitored Test Metrics and Analyzed Effluent Composition as a Function of Time in Interactive PUF Test with Pu Zirconolite-dominant Ceramic

The data in Figure 5 indicate that the WP-14 glass, and perhaps the CPSF5 ceramic, have undergone periodic excursions in reaction rate that are manifested as excursions in effluent pH and electrical conductivity. The excursions in the effluent pH and conductivity continued after the software correction, and so appear to be unrelated to this problem. Similar PUF experiments with several other glass compositions have shown rapid increases in glass corrosion rate occur after certain secondary phases form, such as Na-Ca aluminosilicate zeolites. However, the dissolution rate acceleration was sustained in these cases until complete dissolution of the glass had occurred. However, we have recently started a PUF experiment with a low-activity waste glass formulation (LAWABP1) that has exhibited a similar pattern of transient rate accelerations, as shown in Figure 6. This experiment is being run at twice the flow rate of the PUF test with WP-14 glass/CPSF5 ceramic. Consequently, the peaks during the periodic rate accelerations are broader than in the 1 mL/d test with the WP-14 glass/CPSF5 ceramic. Because the ceramic contains elements that are sparingly soluble under these test conditions, it is highly unlikely that a dissolution rate acceleration of the ceramic could cause the transient marked increases in pH and electrical conductivity. Additional discussion regarding possible cause(s) of the transients observed in the effluent chemistry is provided in the Discussion section under Periodicity in Effluent Chemistry.

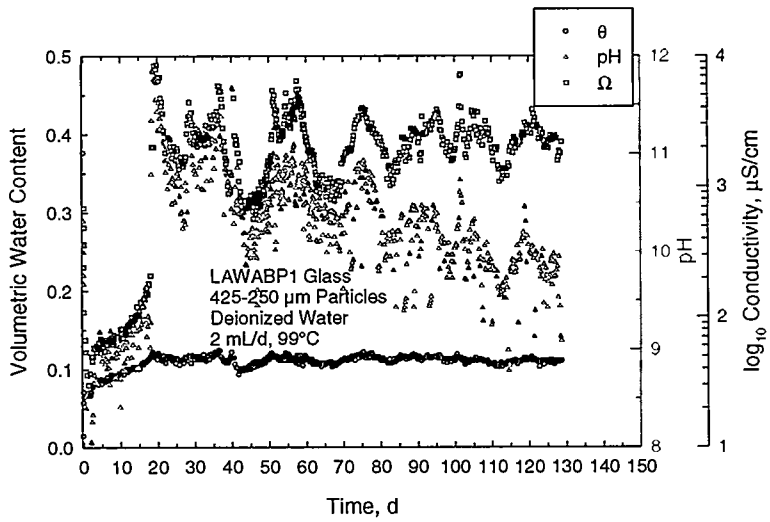

Figure 6. Electronically Monitored Test Metrics in PUF Test with LAWABP1 Glass at 99°C and 2 mL/d Flow Rate

Solution Chemistry

Stable Elements

Results from the ICP-MS analyses of effluent samples are provided in Figure 5b. There is a good correlation between the observed excursions in effluent pH and electrical conductivity with peak concentrations of constituents released from the WP-14 glass and CPSF5 ceramic. There is

also a general trend of decreasing concentrations with increasing reaction time. Unfortunately, there were no elements incorporated in the ceramic to permit unambiguous determination of the dissolution rate as each element is subject to adsorption, ion-substitution, or precipitation in secondary phases. Of the elements, however, Ba is the only element present in the ceramic that is not present in the glass where these effects are minimized. Gadolinium is not present in the glass either but because of its extremely low solubility under the conditions of these tests, it is unlikely to be reliable as a dissolution rate indicator element. Consequently, Ba was used to estimate the ceramic corrosion rate. This is discussed in the Ceramic Corrosion Rate section.

Radioactive Elements

Figure 7 shows the results for total Pu concentration in the effluent as a function of time. The data are highly scattered. However, there is a good correlation between spikes in the effluent pH and Pu concentration. The general trend in the data shows a decrease in Pu release as a function of time. Effluent samples between 300 and 450 d were all near or below the detection threshold, except during the transient pH excursions.

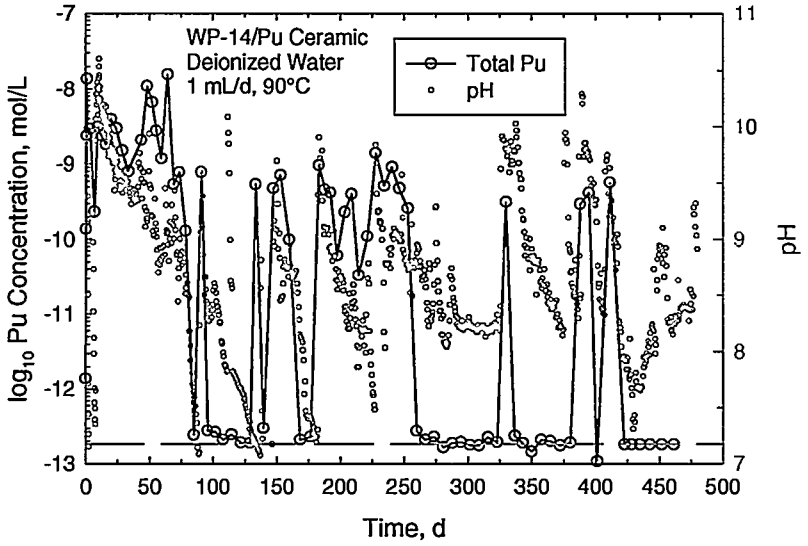

Figure 7. Effluent Pu Concentration as a Function of Time

Filtrations

A comparison of the total measured Pu concentration with the measured concentration after filtration is given in Figure 8. The results show that for

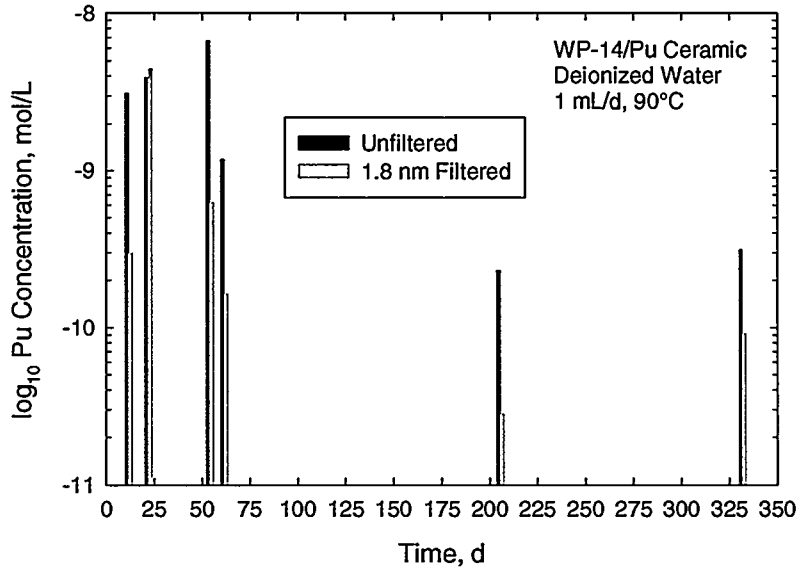

Figure 8. Effect of Filtration on Pu Concentration in Selected Effluents From PUF Test

samples with Pu significantly above the analytical detection threshold, i.e., concentrations between 10^{-10} to 10^{-8} M Pu, a large percentage (>80%) is present in filterable form. Unfiltered samples that analyzed for total Pu near the analytical detection threshold were not filtered; it was assumed that the small amount of Pu present was in soluble form.

The effects of sample reheating on colloidal Pu were also examined on several samples. These samples were divided into three portions. The first portion was left unfiltered, the second portion was filtered at room temperature, and the third portion was reheated to 90°C for 22 hours and then filtered at temperature. On average, 72% of the Pu was removed by cold filtration and 78% by hot filtration. These results indicate that heating of the samples did not redissolve the Pu and so it is unlikely that cooling to room temperature has an effect on the formation of colloidal Pu.

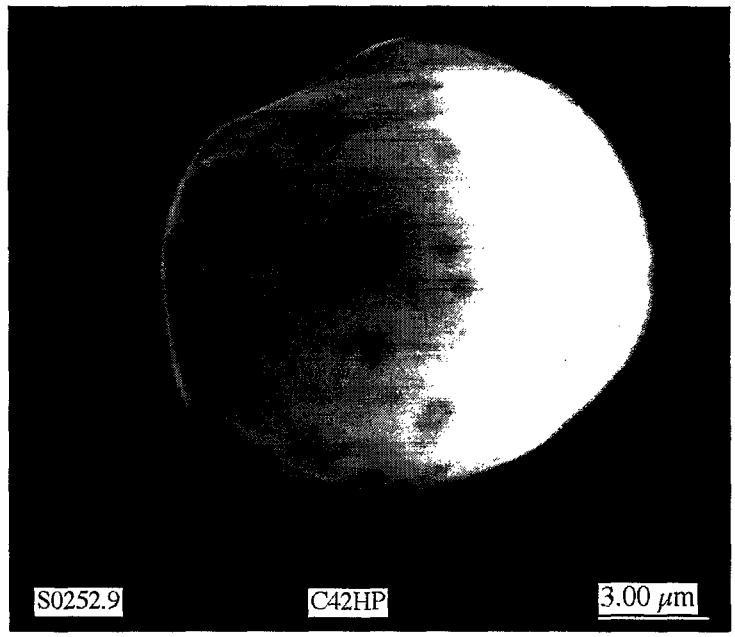

Figure 9. Typical Particle Found on Filters Used to Filter Effluent Samples From PUF Experiment

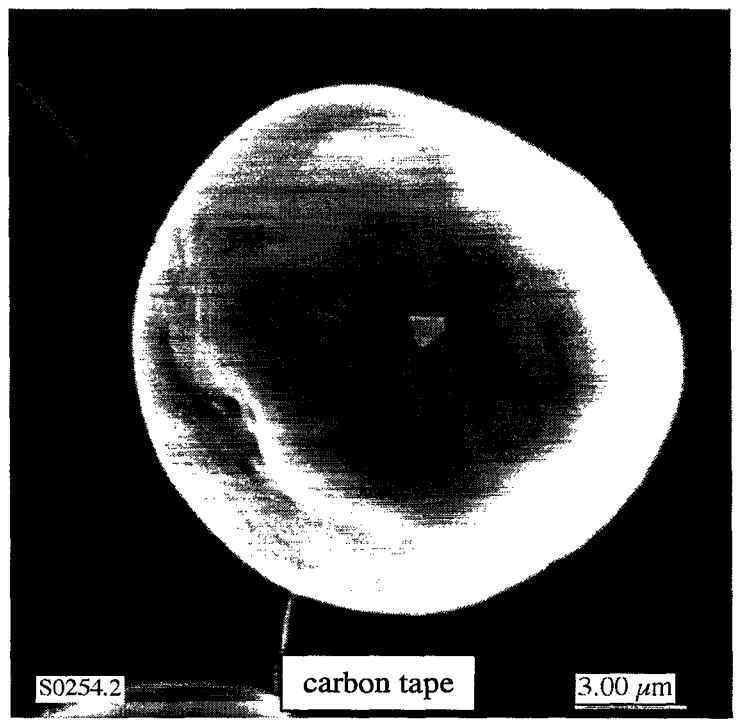

Figure 10. Typical Particle Found on Inside Surface of Ti Plate in PUF Column.

Figure 8 is a SEM photo of a particle typically found on the filters. These particles are far too large to be considered colloids and are far too large to have passed through the porous Ti plate. Instead, these particles likely formed as the water evaporated from the filters. Energy dispersive spectroscopy (EDS) analyses showed that this particle and others

like it are an Al-Ca-Mg-silicate with perhaps some KCl crystals embedded. Leakage of the electrolyte fill solution used in the inline pH sensor into the effluent samples is the likely source of the KCl. In surveys of several filters, a few particles were found on the order of 0.2 μm or less, but these analyzed with similar chemistry to the large particles. No Pu was detected in any of the surveys.

Reacted Solids

SEM Surveys

After the porous plate was removed from the column, carbon tape was used to remove a sample of a fine precipitate layer that coated the inner surface of the plate. Figure 10 shows typical particle morphology. Chemical analysis (EDS) showed that the particle was a simple Na-Mg-silicate, with a few particles having traces of K as well. Again, no Pu could be identified on any of the particles. There is no way to determine if this precipitate layer formed in situ or as a result of cooling and water evaporation.

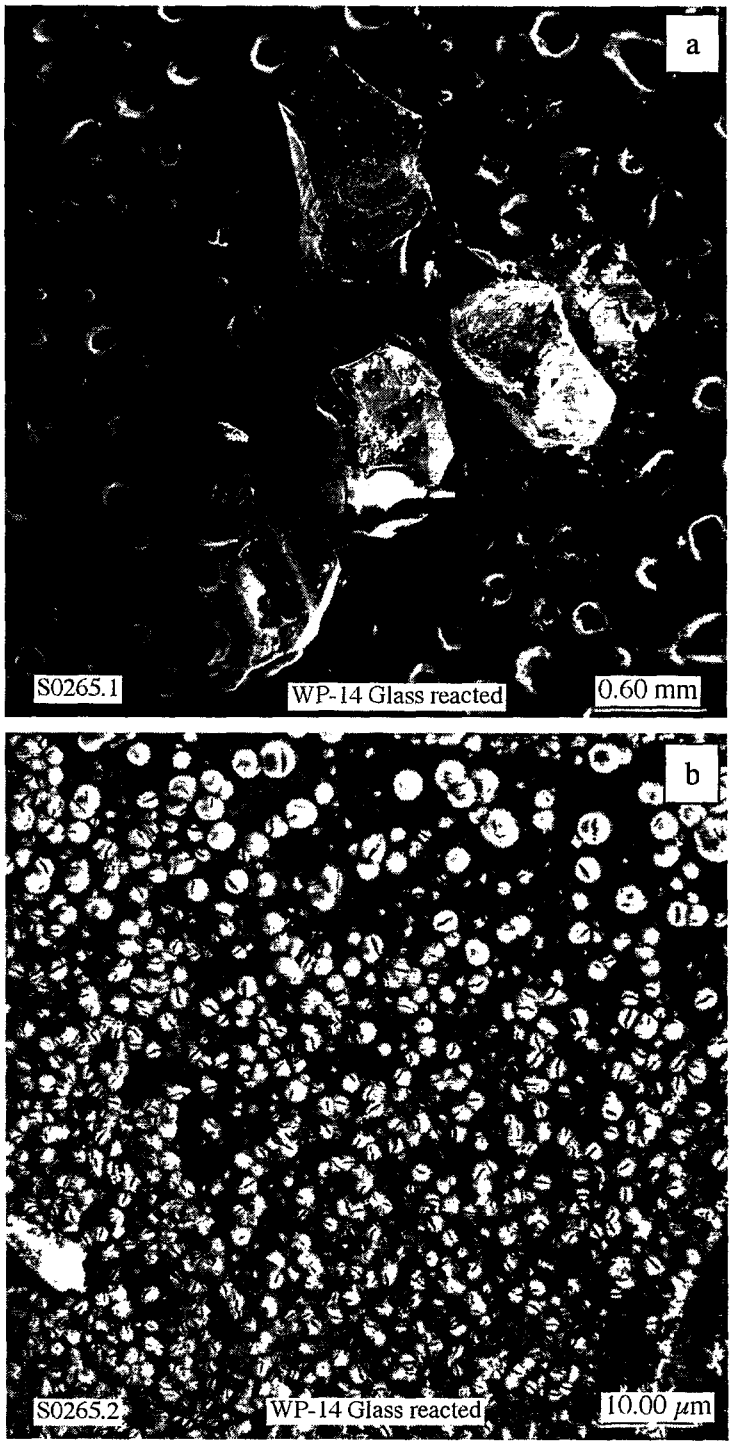

Figure 11. SEM Photos of Reacted WP-14 Glass Grains Extracted From the Bottom of the PUF Column. (Figure 10b is a higher magnification of 10a.)

The SEM analyses of a sample of WP-14 glass removed from the bottom of the PUF column are shown in Figure 11. The photos show that the glass is in good condition with alteration

phases visible only on small portions of the sample surface, exactly as would be expected under the partially saturated conditions of the PUF test. The higher magnification image (Figure 11b) of the alteration phase deposits showed what looks from previous experience to be a clay or amorphous gel-like material. The morphology here though is unusual and striking in that it is studded with hundreds, if not thousands of small spherical particles. Some of these are embedded, or more likely growing out of the gel. Drying of the sample and placing it under high vacuum has clearly ruptured most of the particles. Presumably, sorption of Pu onto these particles is responsible for much of the filterable Pu release observed in the column effluents.

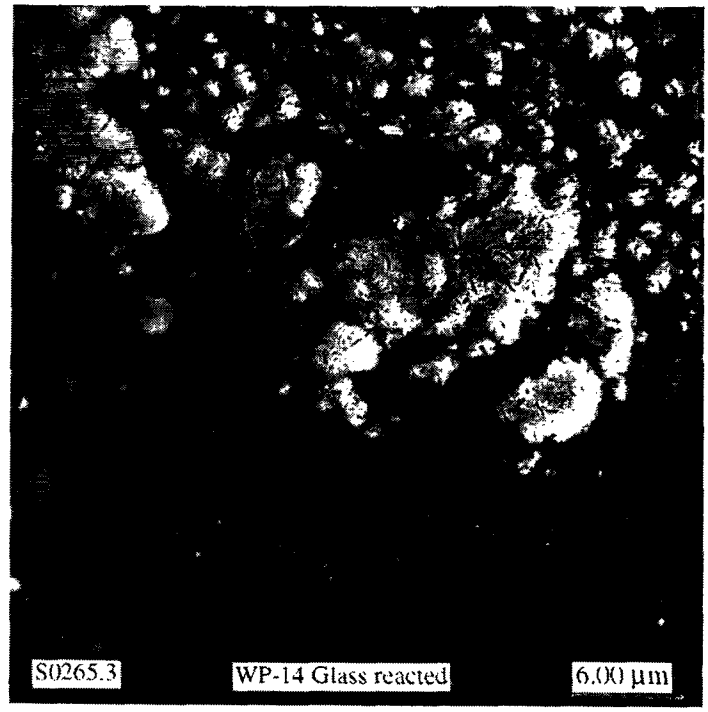

Figure 12. Typical Coating on Glass Particles Removed From the Bottom of the PUF Column

In addition to the particulates, SEM surveys showed numerous deposits with a clay-like morphology, as shown in Figure 12. The EDS analyses showed that the deposit is enriched in Mg relative to the underlying layer. Approximately midway through the bottom glass bed, we also found particles of a phase significantly enriched in Ca and Zr (see Figure 13). TEM-SAED analyses are underway for quantitative identification of these precipitates.

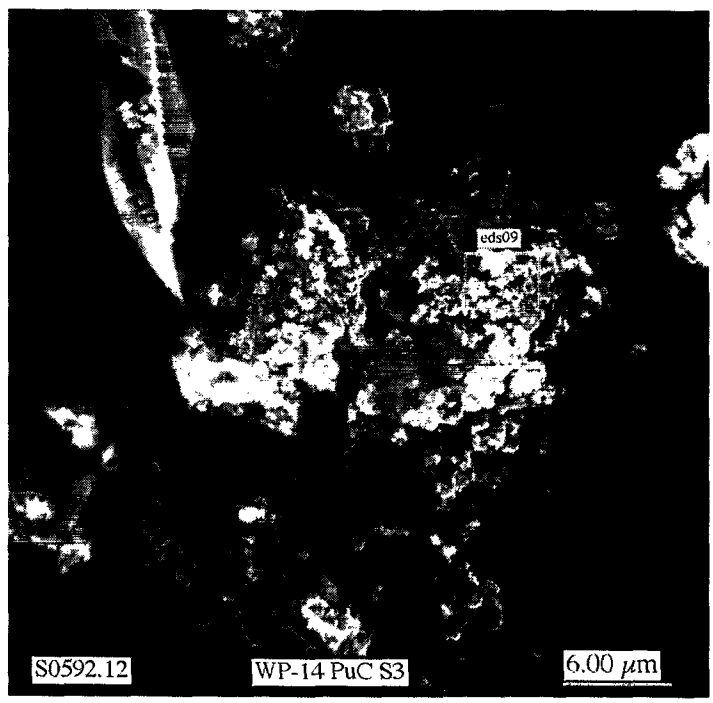

Figure 13. Precipitate Enriched in Ca and Zr as Compared with Underlying Glass. This sample was located near the middle of the bottom glass bed.

Water Mass Distribution

The distribution of water mass associated with the reacted solids, as measured by the mass loss technique described in the PUF Test Procedure section, is provided in Figure 14. The minimum water mass is at the upstream interface between the ceramic and glass beds. Contact angle measurements have shown that the ceramic surface is somewhat hydrophobic relative to the glass. Consequently, the hydraulic mismatch between these materials may be the cause of low water content at this interface. The increasing water mass fraction as a function of depth on the downstream side of the interface is most likely the result of the accumulation of water in the secondary phases discussed in the preceding section and/or because of a change in the water retention characteristic of the glass as secondary phases form on its surface [7].

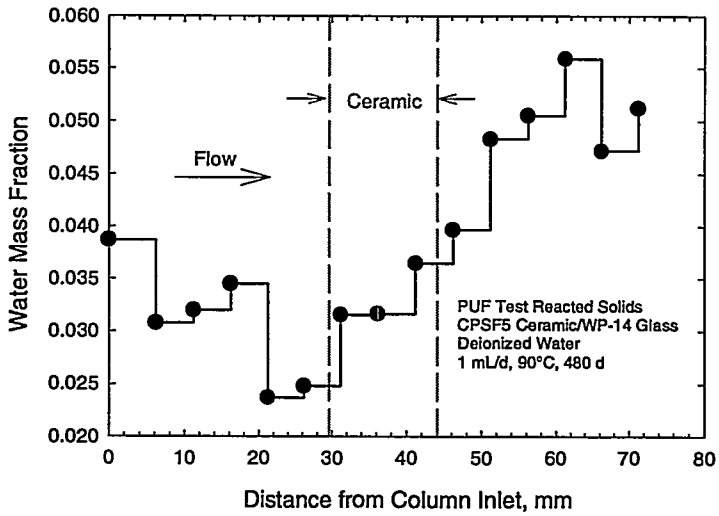

Figure 14. Water Mass Distribution Associated with Reacted Solids After 480 d PUF Experiment

Pu Distribution

A 4 cm² rectangle of double-sided "Very High Bond" tape was placed on a borosilicate glass slide. A portion of the protective liner was removed from the upper surface of the tape to reveal 0.3 cm² of unmasked adhesive. Milligram quantities of dried particles taken at approximately 5 mm intervals were deposited on the unmasked portion of tape. Silicone-coated paper was used to press the particles firmly into the 0.1 cm-thick tape and then the siliconized paper was removed. These samples were then analyzed for ^{239}Pu content with alpha energy analysis (AEA). An Oxford Oasis™ system with eight individual alpha detectors was used. Calibrations were performed for energy and efficiency with geometry identical to that used for the sample mounts and with known activities of analyzed isotopes. Identification and quantification of ^{239}Pu and ^{241}Am was performed using the 5.156MeV peak and 5.486MeV peak, respectively.

Results from the AEA are shown in Figure 15. Despite the highly advection dominant system, the steep ^{239}Pu concentration gradient downstream from the ceramic bed indicates a strong attenuation of Pu in the glass bed with the concentration dropping by two orders of magnitude over a distance of 25 mm. Retention of Pu may be occurring by adsorption from solution, trapping of Pu colloids, or both. It is impossible to distinguish these mechanisms from the AEA data alone but because most all of the Pu exiting the column was found to be colloidal, colloid filtration is probably the more significant retention mechanism. Interestingly, the ^{241}Am data reverse positions with respect to ^{239}Pu on the upstream versus downstream side of the ceramic. Americium is expected to be more soluble and mobile than Pu under these test conditions and the downstream data are consistent with this expectation. The upstream data are more consistent with the original ratio in the ceramic. Because 146 days elapsed between the time when flow and heat were turned off to the column and when the column was dissected, the upstream profile most likely represents a diffusion profile into the glass bed. The mean diffusion penetration depth in 1-D is given by $\sqrt{\pi D_e t}/2$, where D_e is the effective diffusion coefficient. Neglecting chemical retardation, an effective diffusion coefficient of 6×10^{-7} cm^2/s was estimated from the ending volumetric water content in the test (0.15) and the unsaturated diffusive transport curve of Conca, Apted, and Arthur [8]. The mean unretarded penetration depth is then ≈24 mm. Consequently, the upstream data in Figure 15 are consistent with a diffusion profile where the Pu and Am are significantly retarded. The upstream concentration profile was fit with the linear adsorption model in the code CXTFIT [9] and a retardation factor of 156 provided the best fit to the ^{239}Pu data.

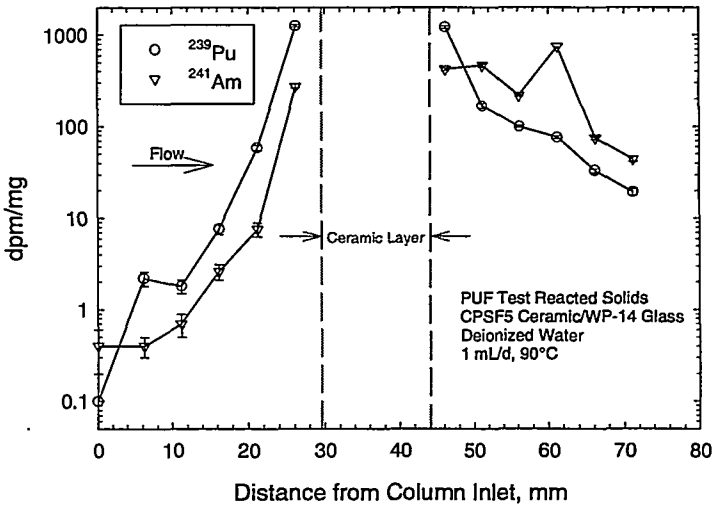

Figure 15. Alpha Energy Analysis of Glass Particles Removed from PUF Column after 480 d of Reaction. For reference, the measured count rate for the CPSF5 ceramic is 1.24×10^7 dpm/mg for ^{239}Pu and 1.77×10^6 dpm/mg for ^{241}Am.

SPFT TEST RESULTS

Flow-Through Rate at 10 mL/d

These experiments were a trial "high-flow" series. This configuration has the advantage of coming to steady-state conditions quickly and maintaining low concentrations of the ceramic components in the effluent, but runs the risk of yielding concentrations of elements in the effluent that are at or near the detection threshold. In this case, typical steady-state concentrations of molybdenum, the key element to index dissolution rates, were <2 parts per billion (ppb). Because the detection threshold for Mo is ~0.1 to 0.2 ppb, most of the concentrations determined in effluent were well within an acceptable range (>3 times the detection threshold).

A plot of the concentration of Mo versus time for the two pyrochlore samples is displayed in Figure 16. At experimental times greater than 60 days, the concentration of Mo is likely to be at or near steady-state conditions, so that apparent dissolution rates can be calculated from Equation (2) above. Because concentrations of Mo and other elements have not been determined for intermediate times, our conclusions concerning these experiments are tentative and await further analysis. However, as will be shown below, the results from these experiments can be compared with the more comprehensive data set representing the experiments with slower flow-through rates (below). One important conclusion to draw from Figure 16 is that concentrations of Mo at the longest experimental duration are approximately the same as those at only two week's dura-

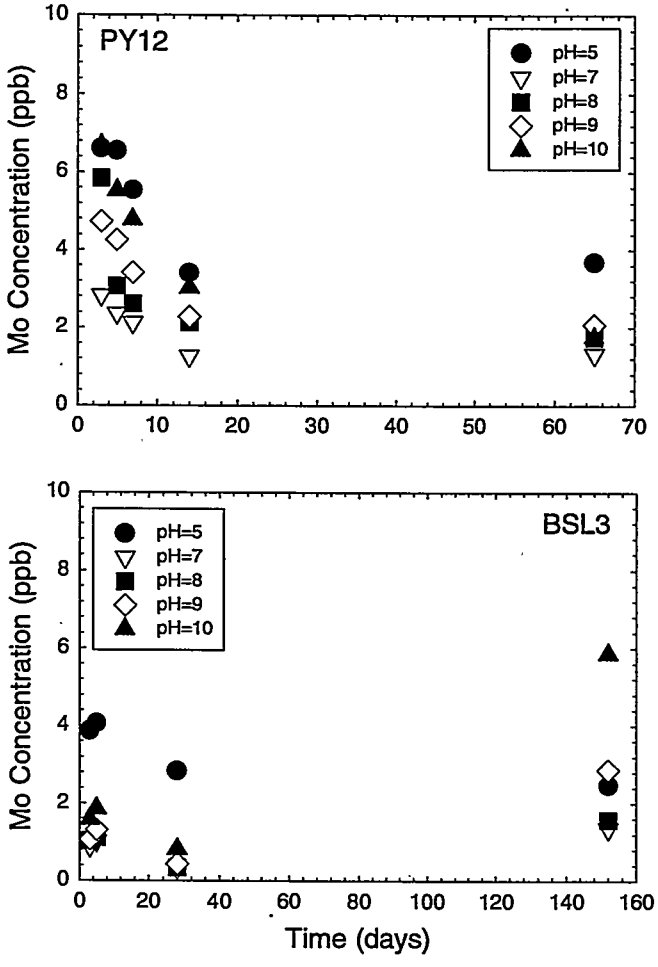

Figure 16. Concentration of Mo vs. Time for PY12 and BSL3 Compositions, T=90°C, Flow-through rate = 10 mL/d

tion. These data would support the preliminary conclusion that Mo concentrations do not decrease continuously over time, but clearly, more data are needed.

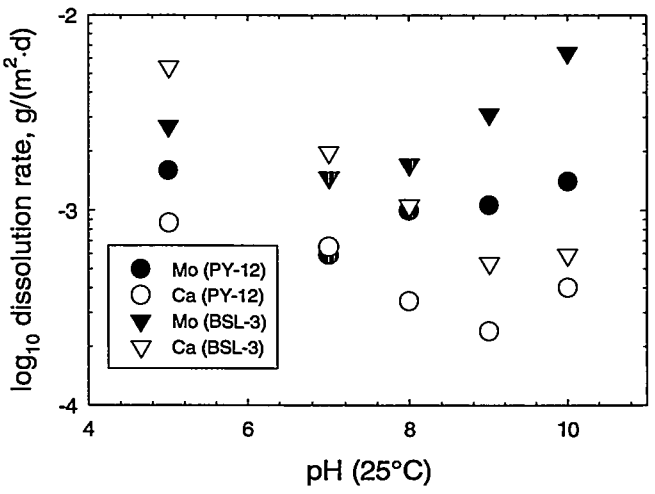

Figure 17. Plot of Dissolution Rate Based on Mo and Ca vs. pH. T = 90°C, Flow-Through Rate = 10 mL/d

Absent from the data displayed in Figure 16 are the concentrations of Mo at pH values of 2. At this value of pH, molybdenum concentrations are at or below the detection threshold, which may indicate the presence of a solid phase that selectively incorporates Mo or the adsorption of Mo onto the ceramic. Because the surface charge on the ceramic is strongly positive at pH 2 and Mo is present as an anion [10] under these test conditions, we believe that adsorption of Mo is likely. A set of batch adsorption experiments is underway to test this hypothesis. Many of the other elements are solubility-limited above pH values of 2; it appears that Ce, Gd, and possibly Ca concentrations are controlled by precipitation reactions and cannot, therefore, be used to determine dissolution rates. Concentrations of Ti and Hf appear to be solubility-limited at every pH value examined. Therefore, it appears that concentrations of Mo are the only viable candidate for determining dissolution rates above pH = 2.

The apparent dissolution rates of the two pyrochlore samples as a function of pH are illustrated in Figure 17. For both samples, there appears to be a dissolution rate minimum near pH values of 7, with the BSL3 sample dissolving at a slightly faster rate than PY12. This

Table 5. Apparent Dissolution Rates (Background Corrected) of Ti-ceramics, 90°C, 2 mL/d Flow-through Rate

Pyrochlore-12 Normalized Dissolution Rates (g/(m²·d))

pH	S (m²)	Ca	Ce	Gd	Mo	Ti
2.0	0.0174	3.40E-04	1.10E-04	8.50E-04		5.00E-06
5.7	0.0178				2.26E-04	
6.7	0.0177				1.45E-04	
8.0	0.0176				1.58E-04	

Baseline-3

pH	S (m²)	Ca	Ce	Gd	Mo	Ti
2.0	0.0172	1.14E-03	6.22E-04	3.80E-04		1.95E-05
5.7	0.0172				1.42E-04	
6.7	0.0174				3.05E-04	
8.0	0.0176				2.10E-04	

Pyrochlore-12 1σ Standard Deviation (g/(m²·d))

pH	S (m²)	Ca	Ce	Gd	Mo	Ti
2.0	0.0174	5.04E-05	1.63E-05	1.27E-05		6.76E-07
5.7	0.0178				3.35E-05	
6.7	0.0177				2.18E-05	
8.0	0.0176				2.35E-05	

Baseline-3

pH	S (m²)	Ca	Ce	Gd	Mo	Ti
2.0	0.0172	1.71E-04	9.30E-05	5.60E-05		2.90E-06
5.7	0.0172				2.13E-05	
6.7	0.0174				4.60E-05	
8.0	0.0176				3.55E-05	

behavior may be expected given that dissolution of TiO_2 polymorphs exhibit amphoteric behavior.

Flow-Through Rate at 2 mL/d

Because effluent concentrations of elements in the experiments with flow-through rates of 10 mL/d were low, we elected to repeat the experiments with slower flow-through rates (2 mL/d).

Experiments with input solutions at pH values of 2, 5.7, 6.7, and 8 are underway and preliminary dissolution rates, based on steady-state concentrations of elements, are listed in Table 5. Concentrations of Ce, Gd, and Ca are well above their respective detection threshold at pH = 2 and concentrations of Mo are easily detected at pH = 5.7, 6.7, and 8. As in the case of the experiments with higher flow-through rates, note that concentrations of Ti and Hf are near or at their respective detection thresholds over the pH interval studied.

Figure 18 displays the concentrations of Ca, Mo, Ce, and Gd at pH = 2 as a function of time for the PY12 and BSL3 ceramic compositions. For the PY12 sample (top diagram), concentrations of Ce and Gd both exhibit an early increase in concentration followed by a smooth, near asymptotic decrease toward what appear to be steady-state values. This behavior is typical for experiments in which the starting powdered materials contain a small number of finer-grained materials or reactive sites (due to grinding and other processing methods) and rapidly react with solution. Once these reactive entities are exhausted, the concentrations of the elements relax towards steady-state values. Another viable interpretation of this

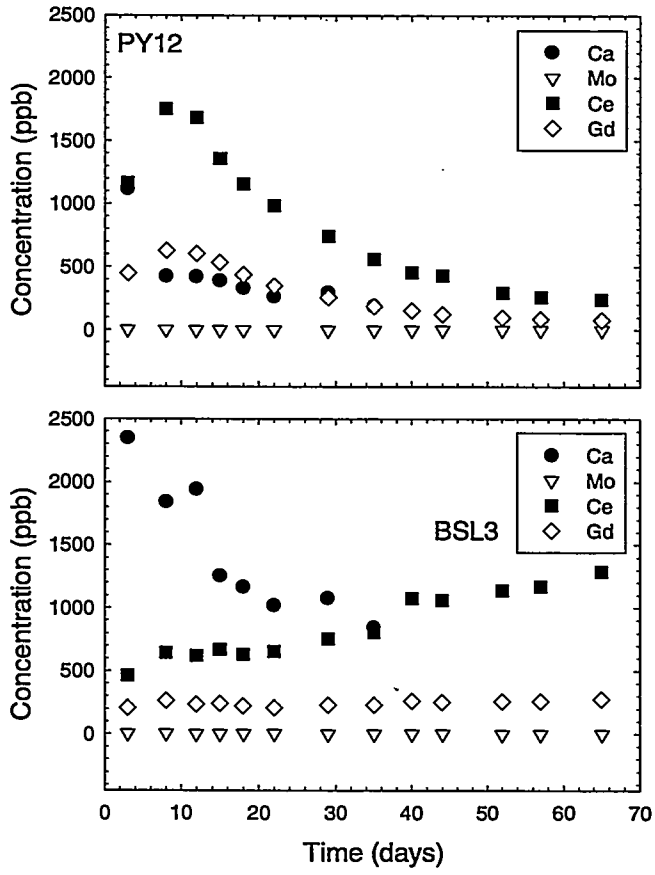

Figure 18. Concentration of Elements vs. Time for PY12 and BSL3 Samples. pH = 2, T = 90°C, Flow-through Rate = 2 mL/d.

behavior is that the surfaces of the ceramic grains begin to form a precipitation or leach layer that effectively mitigates the release of rate-controlling species into solution. The behavior of the elements Ca and Ce in the experiments with BSL3 materials (bottom diagram) is more difficult to reconcile. A rapid increase in Ca concentrations with time, in the manner described above may have occurred too fast to be captured by our sampling interval. The continuous rise in Ce concentrations over the duration of the experiment is unusual, and requires further investigation.

Figure 19 exhibits the concentration of Mo versus time as a function of solution pH. Concentrations of Mo in effluent from experiments with PY12 (top diagram) display some variation, although it appears that steady-state conditions are close to being achieved. The behavior of Mo in experiments with BSL3 is more consistent with steady-state behavior. In both sets of experiments, preliminary apparent dissolution rates can be calculated and the results are listed in Table 5.

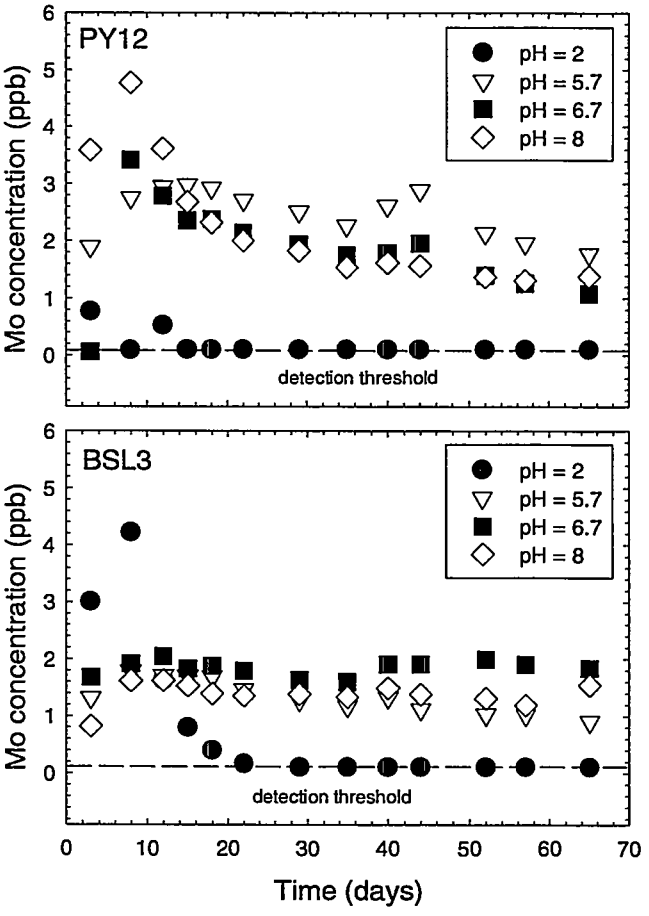

Figure 19. Concentration of Mo vs. Time for PY12 and BSL3 Samples. Variable pH, T = 90°C, Flow-through Rate = 2 mL/d.

Apparent dissolution rates based on preliminary data for Ce, Gd, Ca, and Mo indicate consistent results. Experiments with BSL3 materials at pH values of 5.7, 6.7, and 8 yield rates of 1.4 to 3.1×10^{-4} g/(m^2·d) (based on Mo concentrations). At pH = 2, rates based on Mo concentrations cannot be obtained but apparent rates based on Gd and Ce concentrations are 3.8 to 6.2×10^{-4} g/(m^2·d), respectively. Rates based on Ca are faster, however, at 1.1×10^{-3} g/(m^2·d). In experiments with PY12 ceramic materials, apparent dissolution rates are nearly identical to those calculated for BSL3. Apparent dissolution rates based on Mo concentrations at pH values of 5.7, 6.7, and 8 are 1.5 to 2.3×10^{-4} g/(m^2·d). Rates based upon Ca and Ce concentrations at pH = 2 overlap

with those above with values between 1.1 to 3.4×10^{-4} g/(m^2·d). The rate for PY12 material based on Gd concentrations at pH = 2 are slightly faster (8.5×10^{-4} g/(m^2·d)). For both materials, the apparent dissolution rates based upon Ti concentrations are very slow (5×10^{-6} to 2×10^{-5} g/(m^2·d)), reflecting saturation in a Ti-bearing phase (e.g., rutile, anatase).

Experiments with Ion-irradiated Samples

We have undertaken an additional set of dissolution kinetics studies on similar Ti-based ceramic materials under the auspices of the Environmental Management Science Program [11]. These experiments probe the dissolution rates of $Gd_2Ti_2O_7$ and $Lu_2Ti_2O_7$ monoliths at pH = 2, 90°C with flow-through rates of 4.8 mL/d. For each composition, four monoliths are being tested; two that have been subjected to heavy ion bombardment to simulate radiation damage, and two pristine samples. In these experiments, dissolution rates are calculated based on concentrations of Gd and Lu in the effluent solutions. Because these ceramic materials are similar to those examined under the PIP, we include the results of these experiments to date in this report. Another factor that is relevant to the PIP experiments is that the apparent dissolution rates of the radiation-damaged and the pristine samples can be compared.

Figure 20 illustrates the concentration of Ti and Gd with time for damaged and pristine monoliths of $Gd_2Ti_2O_7$. Because the ion-damaged ceramic materials are amorphous to some depth, the initial releases of Ti and Gd from these samples (Gd-1, Gd-2) are fast. Over time, however, the concentrations of Ti and Gd from the damaged samples approach or overlap with those from the pristine samples (Gd-3, Gd-4). The behavior of Ti and Gd in

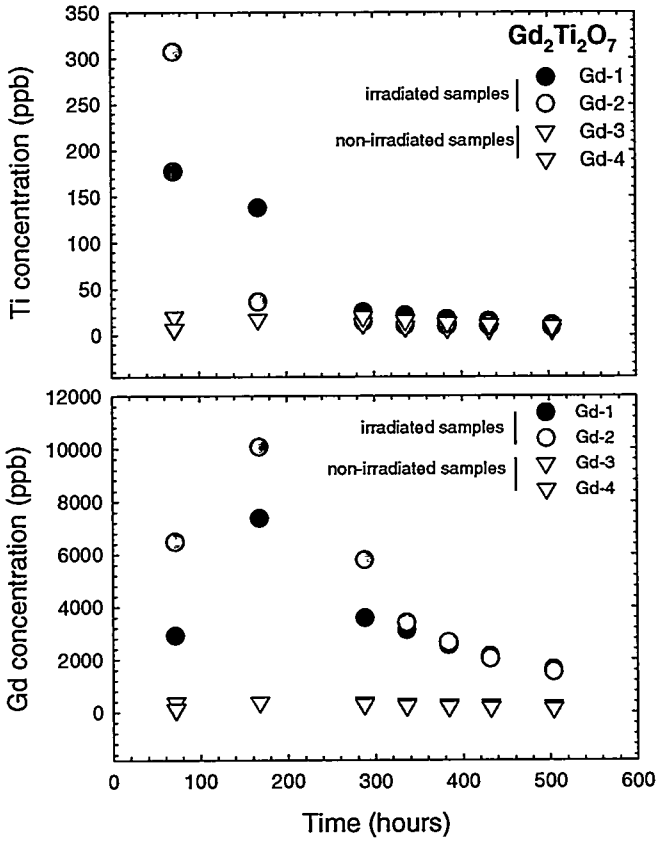

Figure 20. Concentrations of Ti and Gd (ppb) vs. Time. T = 90°C, pH = 2, Flow-through rate = 4.8 mL/d

the amorphous samples indicate that the damaged surface layer has dissolved over the course of the experiment, exposing and dissolving ceramic material unaffected by heavy-ion bombardment. The elements Lu and Ti behave in a similar manner in the experiments with $Lu_2Ti_2O_7$ (Figure 21). The damaged samples (Lu-1, Lu-2) display rapid initial release of Ti and Lu with concentrations relaxing and overlapping with those from the pristine samples (Lu-3, Lu-4). Although tantalizing, it is probably not possible to draw firm conclusions regarding the relative dissolution rates of damaged and pristine samples. Preliminary apparent dissolution rates, based either on Gd or Lu concentrations, indicate values of ~5 to $8x10^{-3}$ g/(m^2·d) ($Gd_2Ti_2O_7$) and ~2 to $5x10^{-3}$ g/(m^2·d) ($Lu_2Ti_2O_7$). Although these apparent dissolution rates are approximately 10 times faster than the rates observed for the PY12 and BSL3 ceramics, one needs to bear in mind that the experiments with Gd and Lu ceramics have not come to steady state. Therefore, the rates will probably continue to decline over time.

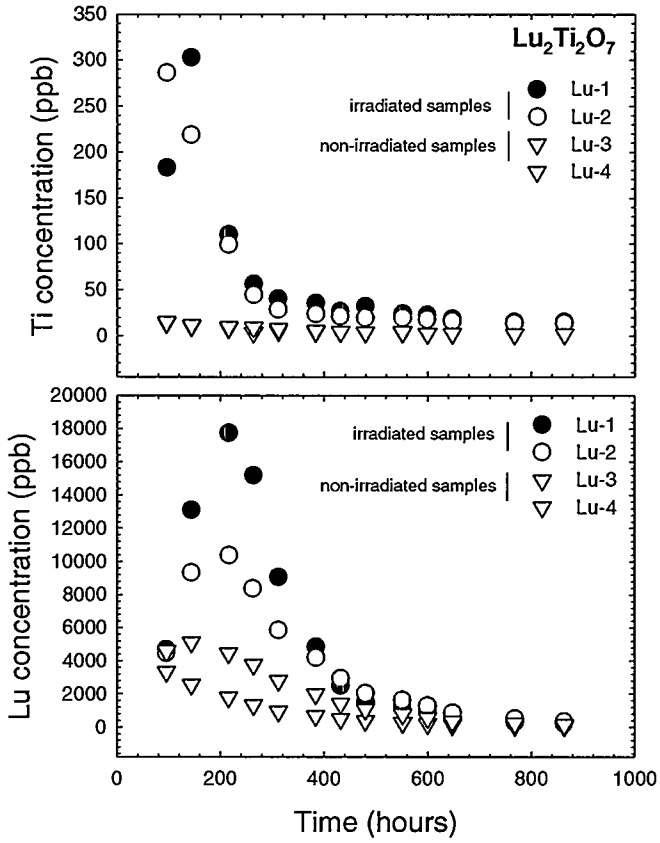

Figure 21. Concentration of Lu and Ti (ppb) vs Time. T = 90°C, pH = 2, Flow-through Rate = 4.8 mL/d

Experiments with Pu-doped Ti-ceramics

Experiments with ^{239}Pu-doped materials (pyrochlore and zirconolite) are currently under way. The experimental conditions are a pH interval of 2 to 12, 90°C, and a flow rate of 2 mL/d. Analyses of the effluent solutions are not yet available. In addition, we are poised to begin dissolution experiments with ^{238}Pu materials under the same experimental conditions.

DISCUSSION

PUF TEST

Although there is no element in the CPSF5 ceramic that could be considered a conservative tracer or marker to determine the ceramic corrosion rate in the PUF test, the best available alternative is Ba. Computation of corrosion rates from PUF test data has not been widely presented, so the procedure will be provided below.

Corrosion Rate Calculation

As in any flow-through column experiment, the calculation of kinetic rates from the effluent composition is more involved than in simpler static experiments. The PUF experimental method introduces one additional complication, in that the water content is also a variable that must be taken into account.

Most experiments with the PUF system are expected to be advection dominated. This can be demonstrated by computing a typical Peclet number for an experiment. The Peclet number (Pe) is given by

$$Pe = \frac{U_p x}{D} \tag{3}$$

where U_p is the pore velocity, x is the distance, and D is the molecular diffusion coefficient of water. In the current experiments, with a volumetric flow rate (q) of 1 mL/d and water content (θ) during the test of approximately 0.1, a typical pore velocity in the test is

$$U_p = \frac{q}{\theta A} = \frac{(1.0\ \text{cm}^3/\text{d})(1.16 \times 10^{-5}\ \text{d/s})}{(0.1)(2.85\ \text{cm}^2)} = 4.07 \times 10^{-5}\ \text{cm/s}. \tag{4}$$

where A is the cross-sectional area of the column. For a column 7.62 cm in length and assuming $D = 10^{-5}$ cm^2/s, this gives a Pe number of

$$Pe = \frac{(4.07\text{E}-05)(3)(2.54)}{10^{-5}} = 30.9. \tag{5}$$

A system with Pe>4 is considered advection dominated, and so the PUF tests clearly fall in this category.

In an advection-dominated system, a one-dimensional steady state-mass balance for any constituent i is given simply by

$$U_d \frac{dc_i}{dx} = \theta \hat{k}_i, \quad x_o \le x \le x_\ell \tag{6}$$

where U_d is the Darcy velocity (m/d), c_i is the concentration (g/m^3), θ is the volumetric water content, $\hat{k}_i$ is volumetric reaction rate (g/m^3· d), x is length (m), x_o is the distance to the start of layer containing the component of interest, in this case the ceramic, and x_ℓ is distance at the end of the layer. The volumetric reaction rate is given by

$$\hat{k}_i = \frac{f_i \frac{\theta}{\varepsilon} S \dot{k}_i}{V_w} \tag{7}$$

where f_i is the mass fraction of element i, ε is porosity, S is the reactant surface area (m^2), $\dot{k}_i$ is the normalized release rate (g/m^2· d), and V_w is the volume of water in a representative elementary volume. It should be noted that in deriving Equation (7), we have assumed that the surface area contacted by condensed water is proportional to the degree of saturation in the column (θ/ε). Substituting Equation (7) into Equation (6), we have

$$U_d \frac{dc_i}{dx} = \frac{f_i \theta^2 S}{\varepsilon V_w} \dot{k}_i \,. \tag{8}$$

We will assume that the chemical changes that occur from the ceramic-water interaction do not effect the corrosion rate of the ceramic and so the $\dot{k}$ is taken as a constant. If we further assume that volumetric water content is approximately uniform throughout the column, we can make use of the following identity

$$\frac{S}{V_w} = \frac{s \cdot m_c}{\theta V_c} = \frac{s(1-\varepsilon)\rho V_c}{\theta V_c} = \frac{s(1-\varepsilon)\rho}{\theta} \tag{9}$$

where s is the specific surface area of the ceramic particles (m^2/g), m_c is the total mass of ceramic in the column (g), V_c is the volume of the ceramic layer (m^3), and ρ is the bulk density of the ceramic (g/m^3). Substituting Equation (9) into Equation (8), we have

$$U_d \frac{dc_i}{dx} = \frac{f_i \theta s (1-\varepsilon)\rho}{\varepsilon} \dot{k}_i. \tag{10}$$

Because the volumetric flow rate (q, m^3/d) is fixed during a PUF test, the Darcy velocity is simply $U_d = \frac{4q}{\pi d^2}$, where d is the column diameter. Integrating Equation (10), we have

$$\frac{4q}{\pi d^2} \int_{c_{ib}}^{c_{iL}} dc_i = \frac{f_i \theta s (1-\varepsilon)\rho}{\varepsilon} \dot{k}_i \int_0^L dx \tag{11}$$

where L is the length of the ceramic bed, c_{ib} is the background concentration of element i, and c_{iL} is the concentration of element i in the effluent from the column. Rearranging the solution to Equation (11), we arrive at the expression we need to calculate normalized release rates from the effluent concentrations

$$\dot{k}_i = \frac{4\varepsilon q (c_{iL} - c_{ib})}{\theta s (1-\varepsilon)\rho \pi d^2 L f_i}. \tag{12}$$

In deriving Equation (12), it has been assumed that no physical or chemical process attenuates the concentration of the component transported away from the ceramic layer. Equation (12) is also only valid for those elements whose source contribution is derived solely from the ceramic. For the present case, that sole element is Ba.

Corrosion Rate Results

Corrosion rate calculations were performed assuming a constant water content value of 0.15, equivalent to the final measured pore saturation of 33.6%. The calculated ceramic corrosion rate as a function of time, using Ba release as the indicator element, is given in Figure 22 along with the computer-

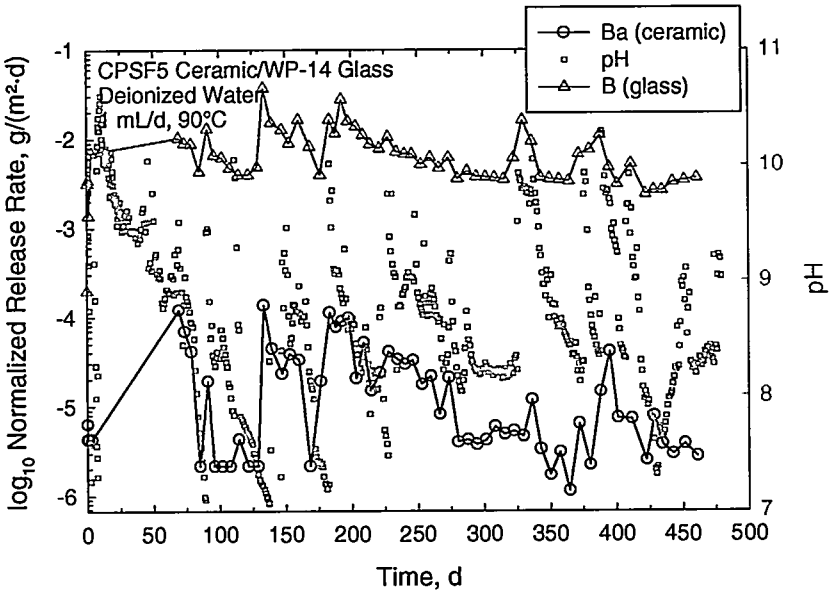

Figure 22. Calculated Corrosion Rate of CPSF5 Ceramic as a Function of Time in Interactive PUF Test

monitored pH data. The corrosion rate of WP-14 glass was calculated from the B concentration data. The results show that the release rate from the ceramic is strongly coupled to the pH excursions observed during the test, as is the glass corrosion rate. Because the pH excursions are controlled by the glass/water reaction, the data show that the performance of the ceramic is directly coupled to the chemical environment imposed by the HLW glass form. However, the overall trend for both forms is a decreasing release rate as a function of time. Moreover, the estimated ceramic corrosion rate from the Ba release is quite low, less than 10^{-5} g/(m^2· d) during the last 200 days of the experiment, except during the pH excursions. The calculated corrosion rate of the WP-14 glass is consistent with rates determined from long-term product consistency tests with SRL-202 glass [12].

Periodicity in Effluent Chemistry

The periodic transients in effluent chemistry illustrated in Figures 4 and 22 are probably the most unusual "feature" of this PUF experiment. As we have not yet completed physical and chemical analyses of the reacted solids removed from the column, we can only offer conjecture as to the potential causes of this phenomenon.

Chemical Hypothesis

As was illustrated in Figure 6, and as we have observed in many other PUF tests with low-activity waste glasses, precipitation of zeolitic alteration phases causes a dramatic acceleration in the corrosion rate of these glasses. The acceleration is detectable exsitu by a rapid increase in effluent pH and electrical conductivity. In some cases, the corrosion rate has been observed to increase autocatalytically back up to the forward rate of reaction of the glass. The forward rate was sustained until either the test was terminated or the column became plugged. However, at least one other LAW glass formulation (LAWABP1) has exhibited transient rate accelerations (see Figure 6) similar to what occurred during the CPSF5/WP-14 interactive test. For the LAWABP1 glass, we believe the rate fails to accelerate autocatalytically because the glass does not supply sufficient amounts of the critical components, Na, Al, and Si, to sustain increasingly rapid zeolite crystallization as the pore fluid pH increases. Consequently, after the initial supersaturation of the system and hence very rapid crystallization occurs, the precipitation rate slows and the glass corrosion rate relaxes back to a new pseudo steady-state condition. However, the

LAW glass continues to corrode at a rate that is higher than before the zeolite precipitation began.

Because the WP-14 glass has 2.5 times less Na than LAW glass, we speculate that not only does zeolite precipitation slow as the pore fluid pH rises after precipitation begins but in fact the precipitation may cease altogether. This should cause the effluent pH to drop back to a nominal value balanced by a much slower rate of glass corrosion. Furthermore, if the high pH pore water composition becomes undersaturated with respect to the zeolite, then the zeolite will begin to dissolve. Dissolution of the zeolite will consume H^+ from the fresh pore water passing through the system. Consequently, the rate of relaxation to a lower pH, lower ionic strength pore fluid composition is dictated by the dissolution rate of the zeolite. Once the pore water pH and composition adjust to where precipitation of the zeolite becomes favorable once again, the cycle repeats.

Hydraulic Hypothesis

Another possible explanation for the observed periodicity is a periodic change in flow path through the column. The effective hydraulic conductivity of an unsaturated medium increases with increasing water content, approximately as the cube of the water content. If there are slight differences in the water content or degree of saturation in the column, something that is quite likely, water will preferentially flow through those areas of higher saturation and conductivity. Higher flux means that the local chemical system in those pores is kept at relatively low reaction progress, so solution concentrations will be low, even though the glass in these regions will be more extensively reacted. Periodically, however, the flow path may change because the accumulation of secondary phases has been shown [7] to alter the hydraulic properties of glasses. The new pathway may have seen little water flux prior to the change, and may, in fact, have been stagnant. Thus, the water present in the pores of the new pathway will have seen a much higher extent of glass reaction and will consequently have a high pH and higher concentrations of dissolved components. The rapid jump to high pH and high effluent concentrations represents the first flushing out of these areas. With time, mass transfer flushes out the stagnant areas and the pH drops. Formation of clay alteration products will also drive the pH down. This continues until the flow paths switch again, and the process repeats itself.

Although both hypotheses above are plausible, the authors believe that the chemical hypothesis is more probable. The principal difficulty with the hydraulic explanation is residence time in the column, which is only approximately 3.5 days. Figure 4 shows that the relaxation time between spikes is on average about 30 to 50 days. Over that time period, 6 to 10 pore volumes will have been exchanged. Consequently, one would expect that the newly accessed stagnant areas would be cleaned out on a much shorter time scale than is observed. Perhaps the flow paths continue to adjust slowly after a major switch in position, and new interconnections are made in the percolation network, connecting new regions of stagnant fluid to the main flow path(s). We are presently assembling a PUF column and supporting hardware that can be imaged with an x-ray microtomograph while an unsaturated flow test is running. By injecting a contrast agent, we will be able to trace the fluid flow path in three dimensions at fine resolution. These experiments should provide clear evidence supporting or contradicting the hydraulic hypothesis.

Colloid Release

The measurement and analysis of colloids was not a major objective of these tests. However, of the analyses that were performed, a significant percentage (>80%) of the Pu released was in colloidal form. This difference is large enough to suggest that the Pu must have traveled in particulate form from the ceramic bed through the glass layer and then exited the column, all under conditions of partial hydraulic saturation. Because of the large advective component applied to the test materials in the PUF system, transport of colloids under unsaturated conditions is to be expected. Unfortunately, there are no details on the size distribution of the colloids to report to help assess the probability of similar colloids moving under the small advective component expected in a waste package.

CONCLUSIONS

PUF EXPERIMENTS

In a 17-month long PUF experiment, a simulated HLW glass and a zirconolite-dominated ceramic for Pu immobilization have been allowed to react in a manner similar to the way they might react in a repository. The results from this experiment have provided several important insights into the long-term release behavior of Pu and neutron absorbers from the ceramic. The results show a strong coupling between the chemistry of the water percolating through a porous bed of the test materials and the corrosion rate of the ceramic. Consequently, should the HLW glass undergo a sustained acceleration in its corrosion rate due to secondary phase formation, the resulting excursion in pH could significantly impact the corrosion rate of the of the ceramic. The 2 to 3 pH unit transient excursions in pH exhibited over the entire course of this PUF experiment, may be caused by the transient acceleration in the glass corrosion rate from the formation of alteration phases or as a result of transient changes in flow paths that occur as the hydraulic properties of the glass change, again due to secondary phase formation. These excursions cause as much as a two order of magnitude increase in the release rate of Ba from the ceramic during these periods. However, in spite of these momentary increases, the overall rate of dissolution of the ceramic remains low. Because of the low emphasis the YMP has placed on HLW glass performance in the repository, the actual long-term behavior of HLW glass in the Yucca Mountain environment remains unclear. Resolution of this issue, however, is beyond the scope of this effort.

For the first 200 days and during pH excursions, Pu was found to be exiting the PUF system primarily as filterable particulates. However, effluent Pu concentrations were found to decrease with time and remained at near detection limits after approximately 250 days, except during transient pH excursions. Similar behavior was observed for the neutron absorber, Gd, with concentrations decreasing to the detection threshold (<0.5 ppb), again except during transient pH excursions. These results indicate that both Pu and Gd will be retained in the can-in-canister waste package to a very high degree. Primarily, this is caused by the formation of highly insoluble secondary phases and/or sequestration by incorporation into or adsorption onto the hydrated

surface layers formed on the HLW glass. A detailed examination of the reacted solids removed from the PUF experiment is underway to help distinguish between these possibilities.

SPFT EXPERIMENTS

The preliminary flow-through data for PY12 and BSL3 at 90°C and pH = 5.7 to 8 indicate nearly identical apparent dissolution rates (1.4 to 3.1×10^{-4} g/(m^2·d)) based on Mo concentrations. At a pH of 2, Mo concentrations appear to be controlled by solubility. Therefore, apparent dissolution rates at pH = 2 are based on concentrations of Ce (1.1 to 6.2×10^{-4} g/(m^2·d)) and Gd (3.8 to 8.5×10^{-4} g/(m^2·d)). Rates based upon Ca concentrations are similar, but exhibit a larger range of values (3.4×10^{-4} to 1.1×10^{-3} g/(m^2·d)). At higher pH values, concentrations of Ce, Gd, and Ca all appear to be affected by precipitation of solid phases; rates based upon these elements are therefore questionable. Both PY12 and BSL3 Ti-ceramic materials exhibit a slightly amphoteric dissolution behavior over the pH-interval examined. The apparent dissolution rates for $Gd_2Ti_2O_7$ and $Lu_2Ti_2O_7$ ($2\text{-}8 \times 10^{-3}$ g/(m^2·d)) are approximately ten times greater than the surrogate materials PY12 and BSL3. However, the experiments with $Gd_2Ti_2O_7$ and $Lu_2Ti_2O_7$ have not exhibited steady-state conditions, so the apparent dissolution rates may continue to decline. The data collectively indicate consistent corrosion behavior of Ti-ceramic materials; yet we cannot definitively state that release of elements into solution is the result of diffusion- or dissolution-controlled processes. Longer experiments and acquisition of activation energy data may resolve this issue.

REFERENCES

1. Cochran, S. G., W. H. Dunlop, T. A. Edmunds, L. M. MacLean, and T. H. Gould. 1997. *Fissile Material Disposition Program Final Immobilization Form Assessment and Recommendation.* Lawrence Livermore National Laboratory, UCRL-ID-128705, Livermore, California.

2. McGrail, B. P., C. W. Lindenmeier, P. F. C. Martin, and G. W. Gee. 1996. "The Pressurized Unsaturated Flow (PUF) Test: A New Method for Engineered-Barrier Materials Evaluation." *Trans. Am. Ceram. Soc.* **72**:317-329.

3. McGrail, B. P., P. F. Martin, and C. W. Lindenmeier. 1997. "Accelerated Testing of Waste Forms Using a Novel Pressurized Unsaturated Flow (PUF) Method." *Mat. Res. Soc. Symp. Proc.* **465**:253-260.

4. Wierenga, P. J., M. H. Young, G. W. Gee, R. G. Hills, C. T. Kincaid, T. J. Nicholson, and R. E. Cady. 1993. *Soil Characterization Methods for Unsaturated Low-Level Waste Sites.* PNL-8480, Pacific Northwest Laboratory, Richland, Washington.

5. American Society for Testing and Materials. 1995. *Standard Test Methods for Determining Chemical Durability of Nuclear Waste Glasses: The Product Consistency Test (PCT).* Standard C1285-94, Philadelphia, Pennsylvania.

6. McGrail, B. P., W. L. Ebert, A. J. Bakel, and D. K. Peeler. 1997. "Measurement of Kinetic Rate Law Parameters on a Na-Ca-Al Borosilicate Glass for Low-Activity Waste." *J. Nuc. Mat.* **249**:175-189.

7. McGrail, B. P, C. W. Lindenmeier, and P. F. Martin. 1999. "Characterization of Pore Structure and Hydraulic Property Alteration in Pressurized Unsaturated Flow Tests." In *Scientific Basis for Nuclear Waste Management XXII*, Editors D. J. Wronkiewicz and J. Lee, Materials Research Society, Warrendale, Pennsylvania.

8. Conca, J. L., Apted, M., and R. Arthur. 1993. "Aqueous Diffusion in Repository and Backfill Environments." *Mat. Res. Soc. Symp. Proc.* **294**:395-402.

9. Parker, J. C., and M. Th. Genuchten. 1984. *Determining Solute Transport From Laboratory and Field Tracer Experiments.* Virginia Agricultural Experiment Station, Bull. No. 84-3. Virginia Polytechnic Institute and State University, Blacksburg, Virginia.

10. Pourbaix, M. 1974. *Atlas of Electrochemical Equilibria in Aqueous Solutions.* English Translation of 1966 French version by J. A. Franklin (Ed.), National Association of Corrosion Engineers, Houston, Texas.

11. Weber, W. 1999. Science to Support DOE Site Cleanup: PNNL Environmental Management Science Program Awards, FY99 Midyear Progress Report, P1.161.

12. Ebert, W. L., and J. K. Bates. 1993. "A Comparison of Glass Reaction at High and Low Glass Surface/Solution Volume." *Nuc. Tech.* **104**:372-384.

DISTRIBUTION

No. of Copies

OFFSITE

2 W. L. Bourcier
Lawrence Livermore National Laboratory
L-219
Livermore, CA 94551

2 H. F. Shaw
Geosciences & Environmental Technology, L-201
Livermore, CA 94551

Peter Gottlieb
TRW
1261 Town Center Dr
Las Vegas, NV 89144

Vijay Jain
Center for Nuclear Waste Regulatory Analyses
Southwest Research Institute
6220 Culebra Road
San Antonio, TX 78238

No. of Copies

ONSITE

U.S. Department of Energy
Richland Operations Office

D. L. Biancosino, K8-50

20 **Pacific Northwest National Laboratory**

J. P. Icenhower, K6-81
V. L. Legore, P8-37
P. F. Martin, P8-37
B. P. McGrail, K6-81 (5)
R. D. Orr, P8-37
H. T. Schaef, K6-81
D. M. Strachan, K6-24 (2)
J. D. Vienna, K6-24
Information Release Office (7)